Kinetics of $O_2(a^1\Delta_g)$ and $I(^2P_{1/2})$ in the Photochemistry of N_2O/I_2 Mixtures†

Valeriy N. Azyazov,‡ Md. Humayun Kabir, Ivan O. Antonov, and Michael C. Heaven*

Department of Chemistry, Emory University, Atlanta, Georgia 30322

Received: October 3, 2006; In Final Form: November 28, 2006

The recent demonstration of a discharge-driven oxygen−iodine laser has generated renewed interest in the kinetics of iodine interacting with electronically excited O_2 and atomic O. Kinetic measurements that are of relevance to the laser have been carried out using 193 nm pulsed laser photolysis of $N_2O/I_2/CO_2$ mixtures. Singlet oxygen was generated in this system by the reaction $O(^1D) + N_2O \rightarrow O_2(a^1\Delta_g, X^3\Sigma_g^-) + N_2$. The fraction of electronically excited O_2 produced by this channel was shown to be >0.9. The secondary photochemistry of the $N_2O/I_2/CO_2$ system was characterized by monitoring the time histories of $I(^2P_{1/2})$, I_2, IO, and $O_2(a)$. Kinetic modeling of these data was used to determine the rate constant for the deactivation of $I(^2P_{1/2})$ by $O(^3P)$ ($k = (1.2 \pm 0.1) \times 10^{-11}$ cm^3 s^{-1}). Quenching of $I(^2P_{1/2})$ by $O(^3P)$ is suppressed in the discharge-driven laser by using NO_2 to scavenge the O atoms. The reaction $O(^3P) + NO_2 \rightarrow O_2 + NO$ is sufficiently exothermic for the production of $O_2(a)$, and it has been speculated that this channel may be significant in the laser excitation kinetics. Photolysis of NO_2 was used to probe this reaction. $O_2(a)$ was not detected, and an upper bound of <0.1 for its production in the reaction of $O(^3P)$ or $O(^1D)$ with NO_2 was established.

Introduction

Reactions between O atoms and iodine-containing molecules have been characterized previously due to the participation of these processes in the chemistry of the atmosphere.[1−3] Additional motivation for studies of these reactions has been provided recently by the demonstration of an oxygen−iodine laser (OIL) that is powered by the electric discharge excitation of O_2 (refs 4−7). The central reaction in the OIL system is energy transfer from singlet oxygen to atomic iodine:

$$O_2(a^1\Delta_g) + I(^2P_{3/2}) \rightarrow O_2(X^3\Sigma_g^-) + I(^2P_{1/2}) \quad (1)$$

The laser operates on the $I(^2P_{1/2}) \rightarrow I(^2P_{3/2})$ transition at 1315 nm. In the following, $I(^2P_{1/2})$, $I(^2P_{3/2})$, and $O_2(a^1\Delta_g)$ are designated by I*, I, and $O_2(a)$, respectively. The chemical kinetics of the electric discharge OIL (EOIL) are significantly different from those of the better-known chemical OIL (COIL).[8−10] This difference arises due to the presence of O atoms in the flow from a discharge singlet oxygen generator. Oxygen atoms are not produced in the chemical generation of $O_2(a)$, but they are present in the flow from a conventional discharge to the extent that the concentrations of $O_2(a)$ and O are comparable.[11] The O atoms have a deleterious effect in the laser system, and their removal by the reaction

$$O + NO_2 \rightarrow O_2 + NO \quad (2)$$

was the key to achieving positive gain in EOIL.[4,5,7] It was postulated that the most important negative effect of the O atoms was the quenching process

$$I^* + O \rightarrow I + O \quad (3)$$

In a related earlier study, Zolotarev and co-workers[12−14] concluded that the presence of O atoms was responsible for the low efficiency of an OIL system that was powered by the photolysis of O_3.

Attempts to measure the rate constant for reaction 3 have resulted in values ranging from $<2 \times 10^{-12}$ (ref 8) to 1.2×10^{-11} cm^3 s^{-1} (refs 7, 11, and 15). Han et al.[8] used the photolysis of $CF_3I/X/N_2O$ and $I_2/X/N_2O$ mixtures (with X = CO_2 or N_2) to investigate reaction 3. The reaction scheme for the I_2 mixtures was as follows:

$$N_2O + h\nu \rightarrow N_2 + O(^1D) \quad (4)$$

$$O(^1D) + X \rightarrow O(^3P) + X \quad (5)$$

$$O(^1D) + N_2O \rightarrow NO + NO \quad (6a)$$

$$\rightarrow N_2 + O_2(a, X) \quad (6b)$$

$$\rightarrow O(^3P) + N_2O \quad (6c)$$

$$O + I_2 \rightarrow I + IO \quad (7)$$

$$O + IO \rightarrow O_2 + I \quad (8)$$

$$O_2(a) + I \rightarrow O_2(X) + I^* \quad (1)$$

Reactions 7 and 8 have near-gas kinetic rate constants ($k_7 = 1.4 \times 10^{-10}$, $k_8 = 1.5 \times 10^{-10}$ cm^3 s^{-1}),[16] so I_2 was rapidly converted to I atoms in the presence of excess O. The kinetics of this system was followed by recording the time-resolved fluorescence from I*. Provided that the O atom concentration was sufficiently high, conditions could be achieved where the long-time fluorescence decay was dominated by reaction 3. Using this approach, Han et al.[8] obtained an upper bound for

† Part of the special issue "M. C. Lin Festschrift".

* Corresponding author. E-mail: heaven@euch4e.chem.emory.edu.

‡ Visiting researcher from the Samara Branch of the P.N. Lebedev Physical Institute.

10.1021/jp066531c CCC: $37.00
Published on Web 01/23/2007

the rate constant $k_3 < 2 \times 10^{-12}$ cm^3 s^{-1}. This was in conflict with the results from a flow tube study[7] and modeling of EOIL,[11] which indicated a rate constant near 10^{-11} cm^3 s^{-1}. Very recently, Azyazov et al.[15] used the photolysis of $O_3/N_2/I_2$ mixtures to examine reaction 3. They obtained a value of 1.2×10^{-11} cm^3 s^{-1}. The accumulated evidence suggests that there were problems with the previous N_2O photolysis experiments. However, if the $k_3 < 2 \times 10^{-12}$ cm^3 s^{-1} upper bound for the rate constant was correct, it is possible that quenching processes that involved the products of O atom chemistry could give the appearance of rapid quenching by O. The present study was carried out to resolve this uncertainty and provide an accurate value of the rate constant for reaction 3. The kinetics of the $I_2/X/N_2O$ system were examined in greater detail by tracking multiple species (I*, I_2, and IO).

The yield of O atoms from N_2O photolysis is of central importance in using the $I_2/X/N_2O$ system to study quenching by O atoms. UV photolysis of N_2O has been widely used as a source of electronically excited oxygen atoms $O(^1D)$, and the photodissociation dynamics of N_2O is of fundamental interest. The reaction of the $O(^1D)$ photofragment with N_2O has three product channels, defined by eqs 6a−c above. It has been extensively studied because one of the products, the NO molecule, plays a role in the depletion of ozone.[17] Marx et al.[18] and Lam et al.[19] reported branching ratios of 0.62 for channel 6a and 0.38 for 6b using photolysis at 184.9 and 206.2 nm. Nishida et al.[20] measured the branching ratio of $O(^3P)$ formation in process 6 to be 0.04 using vacuum-ultraviolet laser-induced fluorescence (LIF) spectroscopy around 130 nm. The IUPAC subcommittee recommends a branching ratio for channel 6c of <0.0086 based on an extensive literature review.[21]

Spin-correlation rules and ab initio calculations[22] for $O(^1D) + N_2O(X^1\Sigma)$ predict that singlet oxygen is the product of reaction 6b, but there has been no direct experimental verification of this expectation. The experiments of Han et al.[8] provide indirect evidence that $O_2(a)$ is formed. As noted above, they observed I* luminescence when $N_2O/CO_2/CF_3I$ or $N_2O/N_2/CF_3I$ mixtures were photolyzed using a 193 nm light, and it was clear from the time evolution that I* was being formed by secondary reactions. In attempts to improve the performance of the OIL powered by O_3 photolysis, Zolotarev et al.[13] tested the use of N_2O, N_2, and/or CO_2 as reagents for the removal of $O(^1D)$, and the best results were obtained for N_2O. Zolotarev et al.[14] concluded that an increase in laser power was achieved due to the fact that N_2O consumes oxygen atoms in process 6 and that $O_2(a)$ is produced by reaction 6b. Note that the yield of $O_2(a)$ from reaction 6b is also of interest from the perspective of atmospheric chemistry. The O_2 $a-X$ emission system is the most intense feature in the Earth's airglow spectrum,[23] and, under certain conditions, reaction 6b could contribute significantly to $O_2(a)$ formation.

To minimize the negative effect of $O(^3P)$ atoms on the performance of EOIL, NO_2 has been added into the post-discharge oxygen to scavenge the excess of oxygen atoms.[5] In modeling this system, Zimmerman et al.[24] found that the improvement in the I* concentration could not be explained by the removal of O atoms alone. An additional source of $O_2(a)$ was needed to achieve agreement with the observed behavior. They speculated that the reaction

$$O(^3P) + NO_2 \rightarrow O_2(a) + NO \qquad (9)$$

may be a contributing factor.[24] The production of $O_2(a)$ by this process has not been reported previously. In the present study, we have searched for evidence of this reaction.

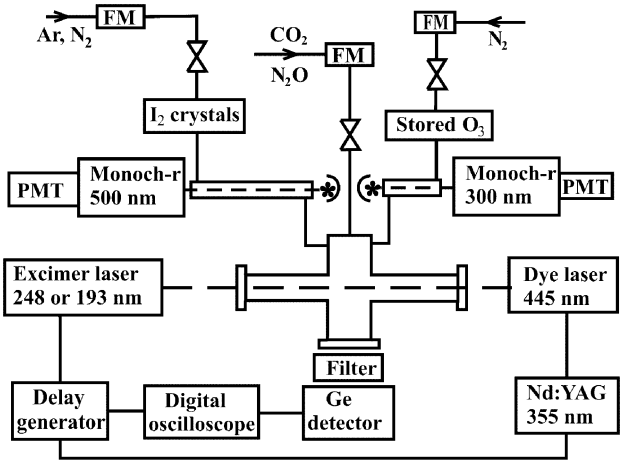

Figure 1. Schematic view of the apparatus.

The measurements reported here began with an investigation of the yield of $O_2(a)$ in reaction 6b. In this work, the photolysis of O_3 was used as a means to calibrate the detector used to measure $O_2(a)$ concentrations. The yield of $O_2(a)$ from reaction 6b was then determined using the photolysis of N_2O/Ar mixtures. Quenching of I* by $O(^3P)$ was examined using the photolysis of $N_2O/CO_2/I_2$/Ar mixtures. The kinetics of $I_2(X)$ removal and IO generation were used to characterize the O atom concentrations. Finally, the photolysis of NO_2 was used to search for evidence of reaction 9.

Experimental

Pulsed laser photolysis techniques were used for all of the kinetic measurements. Emission spectroscopy and LIF were used to follow the time evolutions of ground- and excited-state species. Figure 1 shows a schematic view of the apparatus used in these studies. The photolysis radiation was provided by an excimer laser (Lambda Physik Compex Pro 102, 10 ns pulse duration) operating at 193 nm (ArF) or 248 nm (KrF). The photolysis cell has been described in a recent publication.[15] It was constructed from a solid brass block with 1 cm diameter channels for the flow of gases, the passage of the photolysis and probe laser beams, and the observation of emission from the photolysis zone. To reduce window scattering problems for the photolysis and LIF probe beams, two baffle arms (35 cm long) were attached to the photolysis cell. UV-grade fused silica windows were attached to the ends of both arms. Sets of apertures were mounted inside the baffle arms. In the arm that held the entrance window for the photolysis beam, a cylindrical lens ($f = 20$ cm) was inserted between the apertures, 16 cm away from the photolysis zone. This was used to achieve the optimum photolysis beam size and power density (note that the focus was outside the region viewed by the detector). Emission from photolysis products was recorded at right angles to the axis of the laser beam via a quartz window. The 1315 nm iodine atom emission was selected by a long-pass filter, and the 1268 nm O_2 $a-X$ emission was isolated by an interference filter. These emissions were detected by a high-speed Ge photodetector (ADC 403HS, cooled by liquid N_2). Emission spectra were examined using a monochromator and a slower response but a more sensitive Ge photodetector (ADC 403L). Time-resolved emission signals from the Ge photodetectors were averaged and stored using a digital oscilloscope (Yokogawa DL 1520, 150 MHz response).

The primary gas flow through the photolysis cell consisted of N_2O (or O_3) mixed with Ar and N_2 or CO_2. Metered quantities of iodine were added via a secondary gas flow. I_2 was seeded in this stream by passing Ar, CO_2, and/or N_2 over I_2 crystals at ambient temperature. The I_2 $B-X$ optical absorption at 500 nm was used for concentration measurements. The I_2 and carrier gas mixture was passed through a 1.2 m-long optical absorption cell before entering the photolysis cell. The secondary flow was injected into the $CO_2/N_2O/Ar$ gas mixture via a concentric movable injector. Mixing of the gases occurred during their transportation to the photolysis zone. The distance from the injector to the center of the flow cell could be varied from 1 to 6 cm. The baffle arms of the flow cell were purged using a slow flow of Ar or CO_2. The sample gases N_2O (99.99% purity), Ar (99.998%), CO_2 (99.99%), I_2 (99.8%, Aldrich) were used without further purification. A mass flowmeter (FMA 1814) and needle valves were used to control the gas flow rates. The cell was evacuated by a rotary pump, and the pumping rate was adjusted using a ball valve. Pressures in the fluorescence and absorption cells were measured using capacitance manometers (MKS Baratron models 622 (0−1000 Torr) and 122A (0−10 Torr)).

Ozone was produced by a commercial generator (Pacific Ozone Technology L21) and collected on silica gel cooled to −100 °C. Once a sufficient quantity of ozone had been collected, the silica gel trap was warmed to −70 °C, and the O_3 was eluted by a slow flow of N_2 (0.75 mmol/s). The concentration of ozone was measured by the absorption of light from a mercury lamp near 300 nm.

LIF was used to record the temporal profiles of the I_2 and IO relative concentrations. A Nd:YAG laser (Quanta Ray PDL-2) operating on the second harmonic ($\lambda = 532$ nm) excited the $I_2(B \leftarrow X)$ transition. Re-emitted light around 587 nm was selected by 0.2 m monochromator and detected by a photomultiplier tube. The IO radical was detected via LIF of the $A^2\Pi_{3/2}-X^2\Pi_{3/2}$ transition.[25] A tunable dye laser (Quanta Ray PDL2E) operating near 445 nm was used to excite the 2−0 band. To minimize interference from scattered laser light, LIF was detected via the 2−1 emission band near 458.8 nm. When LIF detection was used, the photolysis and probe laser beams were counterpropagated through the photolysis cell. Fluorescence was collected along an axis that was perpendicular to the laser beams and the gas flow. A UV-blocking filter was placed between the monochromator and the reaction zone to minimize interference from scattering and prompt emissions excited by the photolysis laser (e.g., ion-pair to valence-state emission bands of I_2). A digital delay generator (SRS model DG 535) was used to control the firing of the photolysis and probe lasers.

Results and Analysis

1. $O_2(a)$ Concentration Measurements and the Production of $O_2(a)$ from $O(^1D) + N_2O$. Calibration of the $O_2(a)$ detection system was an essential preliminary for studies of reaction 6b. This was accomplished using 248 nm photolysis of O_3/N_2 mixtures.

$$O_3 + 248\ \text{nm} \rightarrow O_2(a) + O(^1D) \rightarrow O_2(X) + O(^3P) \tag{10}$$

The yield of $O_2(a)$, defined as $\eta_{\Delta,10} = [O_2(a)]/([O_2(a)] + [O_2(X)])$ is close to 0.9 (ref 26). The O_2 $a-X$ emission was monitored at 1268 nm with the slits of the monochromator set to provide a band-pass of about 30 nm fwhm. The trace labeled $I(O_3)$ in Figure 2 shows a typical time-resolved $O_2(a)$ fluorescence intensity signal resulting from the photolysis of O_3. This

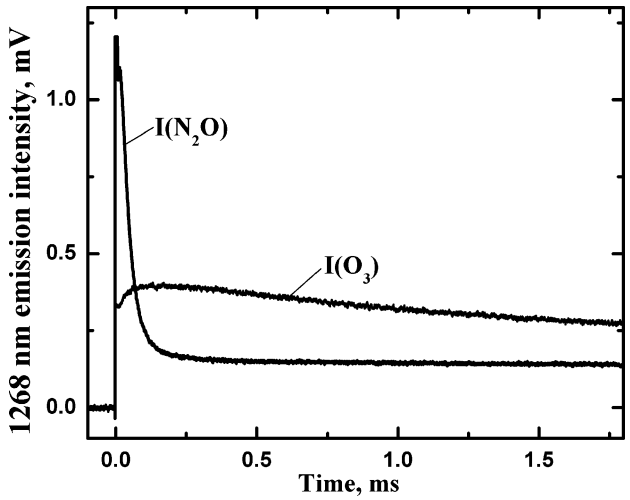

Figure 2. Temporal profiles of the 1268 nm emission intensities for O_3 photolysis ($I(O_3)$) with $P(N_2) = 773.7$ Torr and $P(O_3) = 1.3$ Torr, and N_2O photolysis ($I(N_2O)$) with $P(N_2O) = 207$ Torr and $P(Ar) = 407$ Torr.

trace was obtained at a total pressure of $P(tot) = 775$ Torr with an O_3 partial pressure of $P(O_3) = 1.3$ Torr. The signal level immediately after the photolysis pulse was proportional to the nascent $O_2(a)$ concentration resulting from photolysis. The slight rise in the signal at early times (0.0−0.2 ms) was due to $O_2(a)$ generated by the three-body recombination of O atoms.[17] The subsequent decay was mostly due to quenching by O_3. The number of $O_2(a)$ molecules produced by photolysis is given by

$$N_\Delta(O_3) = \frac{\Delta E_{248}\lambda_{248}}{hc}\eta_{\Delta,10} \tag{11}$$

where ΔE_{248} is the energy absorbed as the laser beam with wavelength $\lambda_{248} = 248$ nm traverses the photolysis zone. A laser power meter (OPHIR 10A-P-V2) was used to measure the energy transmitted by the empty cell (E_0) and the cell with reagent flow (E_a). The absorbed energy ΔE was then calculated from

$$\Delta E = (E_0 - E_a)/(1 - \beta) \tag{12}$$

where β is the loss due to scattering and absorption of the exit window. Typically the energy absorbed by O_3 was in the range of 5−15 mJ per pulse for incident energies in the range of 30 to 50 mJ.

Photolysis of O_3 with He or Ar as the buffer gas was also investigated. With these diluents, the signal at 1268 nm was multiexponential due to contributions from vibrational overtone transitions of OH and electronically excited HO_2. These products were formed by the reaction of $O(^1D)$ with trace quantities of H_2O. This problem was not observed when N_2 was used as the buffer gas, as it is an effective quencher of $O(^1D)$. Note also that the use of high pressures of N_2 in these measurements minimized the local heating caused by the absorption of energy from the photolysis beam. The transient temperature increase did not exceed 30 K.

To observe $O_2(a)$ formation from reaction 6b, mixtures of N_2O in Ar (1:2 ratio) were photolyzed using 193 nm light. The quantum yield for the $O(^1D)$ atoms produced directly by the photolysis of N_2O at 193 nm (eq 4) is close to 0.995 (ref 27). Ar was used as the diluent gas for N_2O because it has a low rate constant for the quenching of $O(^1D)$ (5×10^{-13} cm^3/s, ref 28) as compared to the rate constant for reaction with N_2O ($k_6 = 1.2 \times 10^{-10}$ cm^3 s^{-1}).[21] Emission at 1268 nm was readily

TABLE 1: Representative Data Used for the Determination of $\eta_{\Delta,6b}$

#	$I(N_2O)$, mV	$I(O_3)$, mV	ΔE_{193}, mJ	ΔE_{248}, mJ	$\eta_{\Delta,6b}$
1	0.15	0.35	14.4	11.2	1.03
2	0.15	0.35	15.8	11.2	0.94
3	0.14	0.33	14.2	11.2	1.03
4	0.14	0.51	16	18.4	0.97
5	0.11	0.33	11	11.2	1.05
6	0.1	0.3	9.2	8.4	0.94
7	0.14	0.38	12.6	12.6	1.13
8	0.17	0.54	16.8	16.8	0.97
9	0.072	0.3	6.4	8.4	0.97
10	0.14	0.56	12.6	15.6	0.95

observed following 193 nm photolysis, and the dispersed fluorescence spectrum, observed using the detection of long-lived fluorescence, confirmed that the signal originated from $O_2(a)$. The trace labeled $I(N_2O)$ in Figure 2 shows an example of the time-resolved 1268 nm signal for the photolysis of a N_2O/Ar mixture with $P(N_2O) = 207$ Torr and $P(Ar) = 407$ Torr. The rapidly decaying component at the beginning of this trace (0−0.2 ms) resulted from the formation of electronically excited NO_2 via the three-body reaction

$$O(^3P) + NO + Ar \rightarrow NO_2^* + Ar \qquad (13)$$

NO was present due to reaction 6a, while trace amounts of $O(^3P)$ atoms were produced by photolysis and reaction 6c. Note that extremely small concentrations of NO_2^* could yield signals that were comparable to those from $O_2(a)$ due to the huge difference (a factor of 10^8) in their radiative lifetimes. For the conditions of the measurements reported here, the processes leading to NO_2^* formation were essentially concluded within 0.2 ms of the photolysis pulse. Back extrapolation of the long-lived fluorescence intensity ($t > 0.3$ ms) was used to determine the $O_2(a)$ signal immediately after the photolysis pulse.

The number of $O_2(a)$ molecules generated by the secondary photochemistry for N_2O is given by

$$N_\Delta(N_2O) = \frac{\Delta E_{193}\lambda_{193}}{hc}\gamma_{6b}\eta_{\Delta,6b} \qquad (14)$$

where γ_{6b} is the branching fraction for channel 6b (0.38), and $\eta_{\Delta,6b}$ is the yield of $O_2(a)$ from reaction 6b. As the $O_2(a)$ emission signals were directly proportional to the number of excited molecules generated, eqs 11 and 14 could be combined to give the following expression for $\eta_{\Delta,6b}$ in terms of known and measured parameters:

$$\eta_{\Delta,6b} = \frac{I(N_2O)}{I(O_3)}\frac{\Delta E_{248}\lambda_{248}}{\Delta E_{193}\lambda_{193}}\frac{\eta_{\Delta,10}}{\gamma_{6b}} = 3.08\,\frac{I(N_2O)}{I(O_3)}\frac{\Delta E_{248}}{\Delta E_{193}} \qquad (15)$$

Table 1 shows a representative sampling of the data used to determine $\eta_{\Delta,6b}$ from the fluorescence intensity data. Processing of the complete data set yielded a branching fraction of $\eta_{\Delta,6b} = 1.00 \pm 0.12$, where the uncertainty has been calculated from the range of values obtained using eq 15. Additional systematic errors may be contributed by uncertainties in the previous determinations of $\eta_{\Delta,10}$ and γ_{6b}.

2. Quenching of $I(^2P_{1/2})$ by $O(^3P)$. Photolysis of $N_2O/I_2/CO_2$/Ar mixtures at 193 nm resulted in emission from $I(^2P_{1/2})$ due to the sequence of secondary photochemical reactions listed above (4−8 and 1). The conditions of these experiments were chosen to facilitate observation of the deactivation of I* by $O(^3P)$. I_2 is a rapid quencher of I* (ref 10),

$$I^* + I_2 \rightarrow I + I_2 \qquad (16)$$

while the quenching rate constant for IO is unknown. Hence it was essential to ensure that excess O atoms were generated, so that reactions 7 and 8 went to completion on a time scale that was short compared to the I* fluorescence decay lifetimes, and that there would be sufficient O atoms remaining after the I_2 and IO had been consumed. This entailed using low concentrations of I_2, high pressures of N_2O, and high laser irradiances. As will be shown below, it was possible to operate under conditions where the concentrations of I_2 and IO were reduced to insignificant levels within 200 μs after the photolysis laser pulse, while the I* decay could be observed for at least 1ms. At times beyond 200 μs, an equilibrium between $O_2(a)$ and I* was established between reaction 1 and the back reaction

$$O_2(X) + I^* \rightarrow O_2(a) + I \qquad (17)$$

and the energy was drained from this reservoir primarily through the quenching of I* by $O(^3P)$. The other species that were present in the post photolysis gas mixture (Ar, N_2, CO_2, NO, N_2O, and NO_2) were all inefficient quenchers of $O_2(a)$ and I*.

2.1. I_2 and IO Kinetics. Studies of the I_2 and IO kinetics were carried out to provide quantitative validation of the kinetic model used for the processes leading to $O(^3P)$ formation and verify the rapid removal of I_2 and IO. As described in the experimental section, these species were detected using pulsed LIF. The kinetics of I_2 removal is illustrated by the data shown in Figure 3. These experiments were carried out with a gas mixture consisting of $P(N_2O) = 16.7$, $P(CO_2) = 16.7$, and partial pressure of iodine vapor $P(I_2) = 0.0038$ Torr. I_2 concentration versus time plots are shown for three different photolysis laser irradiances (E, energy per unit area). Note that the first data point in each set was taken with the probe laser firing 1 μs *before* the photolysis laser. This was done to establish the correlation between the LIF signal and the known concentration of I_2 provided by the gas metering system. The next data point in each set was taken with the probe laser firing 1 μs after the photolysis laser. In each case, the drop in I_2 concentration between the first and second data points was too large to be explained by the secondary photochemistry that takes place within the first microsecond. This effect was primarily due to photoexcitation of the I_2 $D-X$ transition followed by collision-induced dissociation of the excited I_2 (ref 29). The absorption cross-section for room-temperature I_2 vapor is 2.1×10^{-17} cm^2 at 193 nm.[29] This transition was saturated for the highest laser intensities used in these experiments. The data for a laser pulse irradiance of $E = 31.5$ mJ cm^{-2} in Figure 3 show a nearly 50% loss of I_2 between the first and second data points. Hence, almost all of the excited I_2 was dissociated during subsequent collisional relaxation processes. This prompt dissociation of I_2 was taken into account in the kinetic model of the photochemistry.

Removal of $O(^1D)$ was very fast on the time scale of these experiments. Reactions 5 and 6 consumed $O(^1D)$ with a first-order decay rate in excess of 10^8 s^{-1}. The rate of I_2 loss after the first microsecond was completely dominated by reaction 7. Numerical simulations of the kinetics (described below) yielded results that were in good agreement with the experimental data. The smooth curves in Figure 3 are examples of the simulations. These calculations were used to determine the concentration of $O(^3P)$ present after the complete conversion of I_2 to I atoms. For example, the concentration of $O(^3P)$ at $t = 50$ μs for the E

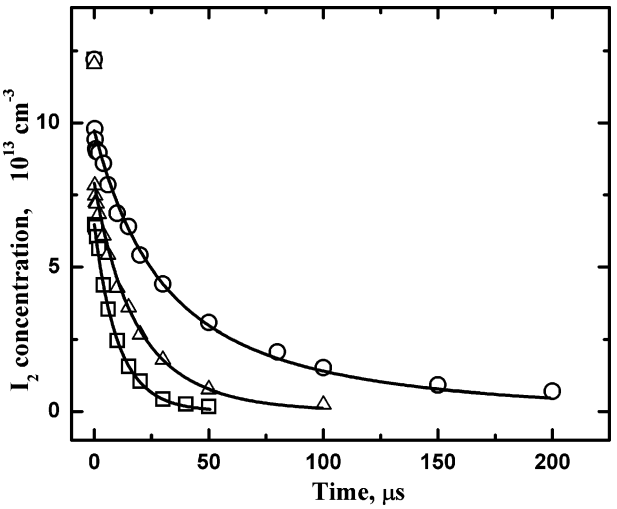

Figure 3. Temporal concentration profiles of I_2 for P(tot) = 50 Torr, $P(CO_2)$ = 16.7 Torr, $P(N_2O)$ = 16.7 Torr, and $P(I_2)$ = 3.8 mTorr. The laser irradiances (E) were (□) 31.5 mJ/cm^2, (△) 18 mJ/cm^2, and (○) 10 mJ/cm^2. The smooth curves were generated by numerical simulations.

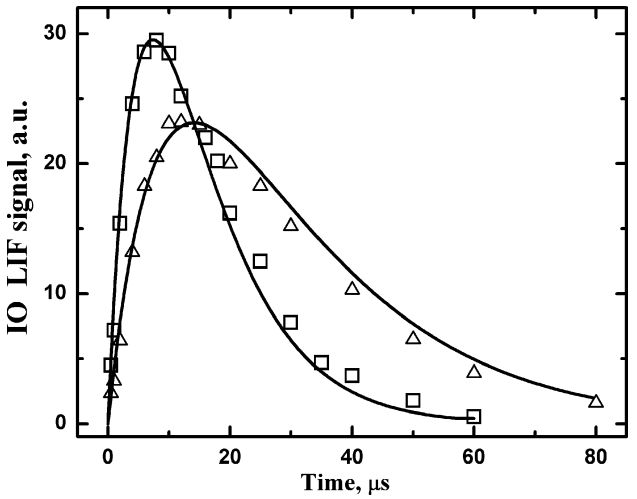

Figure 4. Temporal profiles of IO from the 193 nm photolysis of $N_2O/CO_2/Ar/I_2$ mixtures with P(tot) = 50 Torr, E = 31.5 mJ/cm^2, and $P(I_2)$ = 2.59 mTorr: (□) $P(CO_2)$ = 33.3 Torr, $P(N_2O)$ = 16.7 Torr, (△) $P(CO_2)$ = 16.7 Torr, $P(N_2O)$ = 8.3 Torr. The smooth curves were generated by numerical simulations.

= 31.5 mJ cm^{-2} data shown in Figure 3 was found to be 6 × 10^{14} cm^{-3}. From measurements and simulations, it was established that the conditions for observing the quenching of I* by O(^{3}P) were approximately bounded by $P(N_2O)$ > 10, $P(CO_2)$ > 10, $P(I_2)$ < 0.005 Torr and E > 20 mJ cm^{-2}.

The temporal behavior of IO provided another test of the validity of the kinetic model used in the analysis of the secondary photochemistry. As noted above, it was important to achieve conditions where the IO would not influence the long-time kinetics (t > 100 μs). Gas kinetic rate constants were assumed for the quenching of $O_2(a)$ and I* by IO in establishing the acceptable upper bound for the IO concentration. Figure 4 shows the temporal evolutions of IO for gas mixtures that had two different N_2O pressures, with all other variables held constant. The smooth curves are from numerical simulations. The rapid growth of IO was the result of reaction 7. IO was destroyed by reaction 8 and the processes

$$\mathrm{IO} + \mathrm{IO} \rightarrow \text{products} \qquad (18)$$

$$\mathrm{IO} + \mathrm{NO} \rightarrow \mathrm{I} + \mathrm{NO_2} \qquad (19)$$

When excess O atoms were present, it was noted that the IO concentration reached its maximum value at the point where approximately half of the unphotolyzed I_2 had been consumed. The kinetic model used in simulating the data shown in Figure 4 yielded peak concentrations for IO of 1.5 × 10^{13} cm^{-3}. Even at the maxima, the concentrations of IO generated were not sufficient to compete in the deactivation of $O_2(a)$ or I*.

2.2. I Kinetics.* Experiments designed to characterize reaction 3 were carried out using the photolysis of $N_2O/I_2/CO_2/Ar$ mixtures. I* fluorescence growth and decay curves were recorded with systematic variation of the gas composition and photolysis laser irradiance. Typical results are shown in Figures 5 (CO_2 dependence), 6 (N_2O dependence), and 7 (laser irradiance dependence). Two common features of the I* fluorescence curves are worthy of note. First, there was a prompt I* signal that was almost coincident with the photolysis pulse. This was produced by the 193 nm photolysis of I_2. The fraction of I* produced by this channel was not examined as a separate issue in this work. In the analysis of the I* fluorescence curves, the prompt I* concentration was treated as a variable parameter.

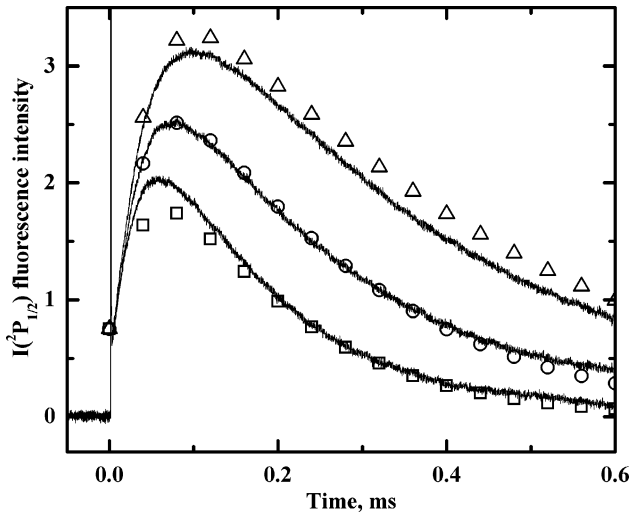

Figure 5. Temporal profiles of the I($^2P_{1/2}$) fluorescence intensity for 193 nm photolysis of $N_2O/I_2/CO_2/Ar$ mixtures with P(tot) = 50 Torr, $P(N_2O)$ = 16.7 Torr, $P(I_2)$ = 4.1 mTorr, and E = 31.5 mJ/cm^2. The carbon dioxide partial pressures $P(CO_2)$ were 8.3 Torr for the upper curve, 16.7 Torr for the middle curve, and 33.3 Torr for the lower curve. The symbols represent simulations for k_3 = 1.2 × 10^{-11} cm^3/s.

It was found that the yield was approximately 25% of the excited I_2 for the conditions used in our measurements. The second significant feature is that the I* fluorescence signals exhibited maxima 100−200 μs after the photolysis laser pulse. As can be seen in Figures 3 and 4, the I_2 and IO were consumed by the time the maximum I* concentration was achieved. Hence, the decay components of the fluorescence curves were suitable for characterizing reaction 3 with minimal interference from competing processes.

Figure 5 shows I* fluorescence profiles for experiments where the laser pulse irradiance of 31.5 mJ cm^{-2} and the pressures of N_2O (16.7 Torr) and I_2 (4.1 mTorr) were held constant. The total pressure was also constant (50 Torr), but the pressures of CO_2 and Ar were varied. The flow rate of the gas mixture depends on the effective molecular weight. Consequently, replacing CO_2 (44 amu) by Ar (40 amu) minimized the perturbation of the flow rate. The flow rate for N_2O was 0.15 mmol/s. Variation of the CO_2 pressure was realized by means of adding metered flows of CO_2 into the N_2O flow. Complete

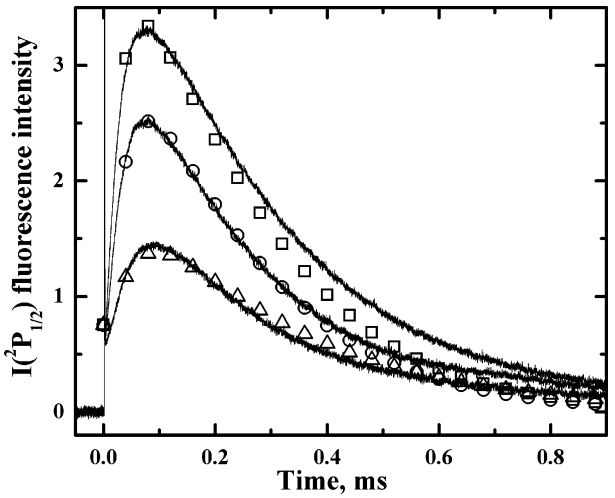

Figure 6. Temporal profiles of the $I(^2P_{1/2})$ fluorescence intensity for 193 nm photolysis of $N_2O/I_2/CO_2/Ar$ mixtures at $P(\text{tot}) = 50$ Torr, $P(CO_2) = 16.7$ Torr, $P(I_2) = 4.1$ mTorr, and $E = 31.5$ mJ/cm^2. The nitrous oxide partial pressures $P(N_2O)$ were 25 Torr for the upper curve, 16.7 Torr for the middle curve, and 8.3 Torr for the lower curve. The symbols represent simulations for $k_3 = 1.2 \times 10^{-11}$ cm^3/s.

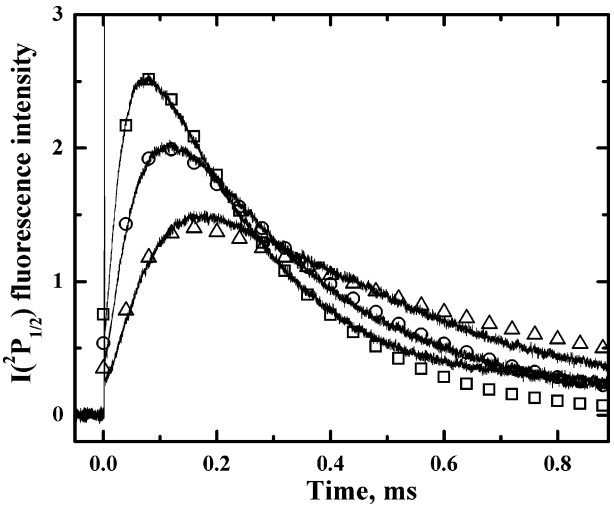

Figure 7. Temporal profiles of the $I(^2P_{1/2})$ fluorescence intensity for 193 nm photolysis of a $N_2O/I_2/CO_2/Ar$ mixture with $P(\text{tot}) = 50$ Torr, $P(N_2O) = 16.7$ Torr, $P(CO_2) = 16.7$ Torr, and $P(I_2) = 4.1$ mTorr. The laser irradiances were 31.5 mJ/cm^2 for the upper curve, 18 mJ/cm^2 for the middle curve, and 10 mJ/cm^2 for the lower curve. The symbols represent simulations for $k_3 = 1.2 \times 10^{-11}$ cm^3/s.

mixing of N_2O and CO_2 occurred during passage through the 0.25 in. o.d. tubing that carried the gas mixture to the photolysis cell. I_2 vapor was transported to the photolysis cell using CO_2 as the carrier gas with a flow rate of 0.074 mmol/s. CO_2 was also used as the purge gas for the baffle arms at a flow rate of 0.074 mmol/s.

CO_2 relaxes $O(^1D)$ to $O(^3P)$ and thereby controls the concentration of $O_2(a)$ produced via reaction 6b. This is the primary reason for the decrease in the I* signal with increasing CO_2 pressure that is evident in Figure 5. These data provide a useful insight concerning the source of $O_2(a)$. In a previous study of this photochemistry, Han et al.[30] speculated that $O_2(a)$ might be generated by reaction 8 ($O(^3P) + IO$). If this reaction were of importance, the addition of CO_2 would increase the I* signal. From the data in Figure 5 and from kinetic modeling of the full data set (described below), we conclude that the branching fraction for production of $O_2(a)$ from reaction 8 is low (<0.1).

The I* fluorescence signals shown in Figure 6 illustrate the effects of changing the N_2O pressure. Here the N_2O/Ar pressure ratio was manipulated to maintain a constant total pressure. Increasing N_2O at a constant laser irradiance had the effect of increasing the concentrations of the secondary products $O(^3P)$ and $O_2(a)$. This in turn increased I* and the rate of I* formation. As can be seen in Figure 7, similar effects were observed when the laser irradiance was varied while the gas composition was held constant.

3. Numerical Simulation. Kinetic modeling was used to analyze the time histories of I*, I_2, and IO. The reactions and rate constants used in this model are listed in Table 2. The $O_2(a)$ branching fraction for reaction 6b, determined in the present study, was set to 1.0. The system of coupled differential rate equations was solved using the FEMLAB 3.1 modeling package. The initial concentrations of oxygen atoms were adjusted so that the measured I_2 decays were accurately reproduced. The initial I_2 concentration before the photolysis pulse, $N^b(I_2)$, was determined from the absorption cell measurements. The concentration of I_2 present after the pulse, $N^a(I_2)$, was determined from measurements of the type illustrated by Figure 3. The total iodine atom (I and I*) concentration immediately after the laser pulse was $2(N^b(I_2) - N^a(I_2))$, and the branching fraction for the production of I* was found to be 0.25. Simulations of the full set of data for I*, I_2, and IO were used to obtain an optimum value for the rate constant for quenching of I* by $O(^3P)$. The system was found to be well constrained, yielding a rate constant of $k_3 = (1.2 \pm 0.1) \times 10^{-11}$ cm^3 s^{-1}. The smooth curves in Figures 3 and 4 and the symbols in Figures 5, 6, and 7 are the results of simulations that employed the best-fit value for k_3.

TABLE 2: Rate Constants Used in the Kinetic Model for $N_2O/I_2/CO_2$ Photochemistry at $T = 300$ K

reaction	rate constant, cm^3/s	ref
6a, $O(^1D) + N_2O \rightarrow NO + NO$	7.2×10^{-11}	21
6b, $O(^1D) + N_2O \rightarrow O_2(a) + N_2$	4.4×10^{-11}	21
6c, $O(^1D) + N_2O \rightarrow O(^3P) + N_2O$	1×10^{-12}	21
1, $I + O_2(a) \rightarrow I^* + O_2(X)$	7.6×10^{-11}	10
17, $I^* + O_2(X) \rightarrow I + O_2(a)$	2.7×10^{-11}	10
7, $O + I_2 \rightarrow I + IO$	1.4×10^{-10}	16
8, $O + IO \rightarrow O_2 + I$	1.5×10^{-10}	16
3, $I^* + O(^3P) \rightarrow I + O(^3P)$	1.2×10^{-11}	this work
5, $O(^1D) + CO_2 \rightarrow O(^3P) + CO_2$	1.3×10^{-10}	21
5, $O(^1D) + Ar \rightarrow O(^3P) + Ar$	5×10^{-13}	21
16, $I^* + I_2 \rightarrow I + I_2$	3.8×10^{-11}	10
18, $IO + IO \rightarrow$ products	9.9×10^{-11}	31
19, $IO + NO \rightarrow I + NO_2$	1.95×10^{-11}	31
$I^* + O_2(a) \rightarrow I + O_2(b)$	1.1×10^{-13}	10
$I^* + O_2(a) \rightarrow I + O_2(a)$	1.1×10^{-13}	10
$I^* + N_2O \rightarrow I + N_2O$	2.1×10^{-15}	30
2, $O(^3P) + NO_2 \rightarrow NO + O_2$	9.7×10^{-12}	21

4. Search for Evidence of $O_2(a)$ from $O + NO_2$. Pulsed photolysis of NO_2 was used to search for evidence of $O_2(a)$ formation from reaction 2. Photolysis using both 248 and 193 nm light was investigated. The absorption cross-sections of the dimer N_2O_4 at these wavelengths were much greater than those of NO_2, and dimers absorbed a considerable fraction of the laser radiation when the experiments were carried out at room temperature. To minimize the concentration of N_2O_4, the photolysis cell was heated to 350 K, and the pressure of NO_2 was kept below 50 Torr. The temperature of the gas was measured by a thermocouple located at the exit of the photolysis zone. Photolysis of NO_2 at 248 nm simplifies the kinetics, as the only dissociation products are $O(^3P)$ and NO. However, the absorption cross-section at this wavelength is relatively small.

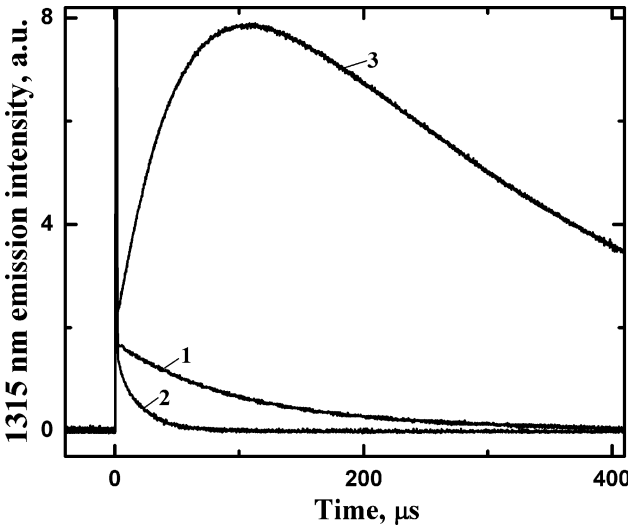

Figure 8. Time-resolved I*−I emission for 193 nm photolysis of NO_2 or N_2O in the presence of I_2. Ar and N_2 were used as buffer gases. These measurements were for a total pressure of 36 Torr with $P(I_2) =$ 13.9 mTorr. Curve 1 was for a mixture of Ar (18 Torr) and N_2 (18 Torr). The I* emission was from direct photolysis of I_2. Curve 2 was for a mixture of NO_2 (18 Torr) and Ar (18 Torr), which does not show any evidence of enhanced I* production. Curve 3 was for a mixture of N_2O (18 Torr) and N_2 (18 Torr), which shows the expected I* enhancement resulting from photochemical $O_2(a)$ production.

Attempts to observe O_2 $a-X$ emission at 1268 nm following 248 nm photolysis of NO_2/Ar mixtures were unsuccessful. Switching to 193 nm photolysis of NO_2 offered the advantage that the absorption cross-section is much greater than that for 248 nm. However, $O(^3P)$ and $O(^1D)$ are produced with branching fractions of 0.45 and 0.55, respectively.[32] This opened the possibility of observing $O_2(a)$ from both reaction 2 and the reaction of $O(^1D)$ with NO_2. To examine the production of $O_2(a)$ from process 2 alone, N_2 was added to convert nascent $O(^1D)$ to $O(^3P)$. A wide search of the parameter space yielded no evidence for $O_2(a)$ formation using 193 nm light to initiate the chemistry. The sensitivity of the apparatus was such that a detectable signal would have been produced if the branching to $O_2(a)$ exceeded 10%.

The primary difficulty in these measurements was the weakness of the O_2 $a-X$ transition, which has a radiative lifetime of 76 min.[33] A further search for evidence of $O_2(a)$ formation was made using energy transfer to I* (0.13 s radiative lifetime) as an indirect detection method. Photolysis of NO_2/I_2/Ar mixtures generates I atoms by direct excitation and through reactions 7 and 8. These atoms could then be excited by $O_2(a)$ resulting from reaction 2. Figure 8 shows I* fluorescence curves recorded for the photolysis of I_2 in mixtures of Ar and N_2 (curve 1) and NO_2/Ar (curve 2). Quenching of I* by I_2 determined the fluorescence decay rate of curve 1. The decay of curve 2 was faster due to quenching by the $O_2(X)$ from reaction 2. Clearly there was no evidence for excitation of I* by $O_2(a)$. Curve 3 was simply a check of the system where NO_2 was replaced by N_2O. From these measurements, we conclude that the yield of $O_2(a)$ from reaction 2 or the reaction $O(^1D) + NO_2$ is insignificant.

Discussion

It was found that the O_2 produced by the reaction of $O(^1D)$ with N_2O is almost entirely $O_2(a)$, as expected on the basis of spin correlation rules. Hence, the branching fraction for reaction 6b (0.38) is also the branching fraction for the production of $O_2(a)$ from reaction 6. The relatively high yield of $O_2(a)$ raises the possibility that reaction 6 may contribute to the Earth's airglow. Confirmation that $O_2(a)$ is produced by $O(^1D) + N_2O$ also explains the results of Zolotarev et al.[13,14] who found that adding N_2O to I_2/O_3 mixtures improved the performance of the photolysis-initiated laser. It will be of interest to re-evaluate the potential of this type of device using the branching fraction and rate constant data determined in this study.

The rate constant for quenching of I* by $O(^3P)$ obtained in this work was in excellent agreement with the results from a study of $I_2/O_3/X$ photochemistry.[15] It is also in agreement with estimates for k_3 obtained by modeling EOIL device performance.[7,11] However, these results did not agree with earlier work from our laboratory,[8] where studies of the $N_2O/I_2/X$ photochemistry yielded an upper bound for k_3 of $<2 \times 10^{-12}$ cm^3 s^{-1}. It is difficult to pin point the problems with the earlier experiments, but it seems likely that the estimates of the O atom concentrations were in error. These densities were estimated on the basis of the absorbed energy, without the additional cross-checks provided by observing the I_2 and IO kinetics.

The large rate constant for the quenching of I* by $O(^3P)$ suggests that a Landau−Zener curve-crossing mechanism is involved. This is similar to the situation for the quenching of I* by $Cl(^2P)$, which occurs with a room-temperature rate constant of 1.5×10^{-11} cm^3 s^{-1} (ref 34). In the case of I* + Cl, it was possible to identify the specific curve crossing that dominated the quenching process using the results from high-level theoretical calculations.[34] Ab initio potential energy curves for I + O and I* + O were reported by Roszak et al.[35] Figures 2 and 3 in their paper show several avoided crossings (which become curve crossings in a diabatic representation) that could be responsible for the fast quenching.

The deleterious effect of O atoms on the discharge-driven OIL are clearly seen to be a consequence of the direct quenching of I* by O atoms. The addition of NO_2 to the post-discharge oxygen flow improves the laser by scavenging O, but there is no evidence to support the tentative suggestion that $O_2(a)$ is generated during the scavenging process. The present measurements show that the yield of $O_2(a)$ from $O + NO_2$ is insignificant. There is, however, another way in which the removal of O atoms may benefit the laser. Vasiljeva et al.[36] reported that the three-body quenching process $O + O_2(a) + O_2 \rightarrow 2O_2 + O$ occurs with a rate constant of approximately 10^{-32} cm^6 s^{-1}. Hence, removal of the O atoms may also decrease the rate of $O_2(a)$ deactivation.

Acknowledgment. We are grateful to W. Solomon and D. Carroll (CU Aerospace), S. Davis and T. Rawlins (PSI, Inc.), and G. Perram (AFIT) for many helpful discussions concerning the kinetics of oxygen discharges and discharge-driven iodine laser systems. This work was supported by the Air Force Office of Scientific Research through a Multidisciplinary Research Initiative (Grant F49620-01-1-0357).

References and Notes

(1) Bedjanian, Y.; Poulet, G. *Chem. Rev.* **2003**, *103*, 4639.

(2) Carlos Gomez Martin, J.; Spietz, P.; Burrows, J. P. *J. Photochem. Photobiol., A: Chem.* **2005**, *176*, 15.

(3) Stutz, J.; Hebestreit, K.; Alicke, B.; Platt, U. *J. Atmos. Chem.* **1999**, *34*, 65.

(4) Carroll, D. L.; Verdeyen, J. T.; King, D. M.; Zimmerman, J. W.; Laystrom, J. K.; Woodard, B. S.; Benavides, G. F.; Richardson, N. R.; Kittell, K. W; Solomon, W. C. *IEEE J. Quantum Electron.* **2005**, *41*, 1309.

(5) Carroll, D. L.; Verdeyen, J. T.; King, D. M.; Zimmerman, J. W.; Laystrom, J. K.; Woodard, B. S.; Benavides, G. F.; Kittell, K. W.; Solomon, W. C. *IEEE J. Quantum Electron.* **2005**, *41*, 213.

(6) Carroll, D. L.; Verdeyen, J. T.; King, D. M.; Zimmerman, J. W.; Laystrom, J. K.; Woodard, B. S.; Benavides, G. F.; Kittell, K.; Stafford, D. S.; Kushner, M. J.; Solomon, W. C. *Appl. Phys. Lett.* **2005**, *86*, 111104/1.
(7) Rawlins, W. T.; Lee, S.; Kessler, W. J.; Davis, S. J. *Appl. Phys. Lett.* **2005**, *86*, 051105.
(8) Han, J.; Tinney, S. P.; Heaven, M. C. *Proc. SPIE-Int. Soc. Opt. Eng.* **2004**, *5448*, 261.
(9) Heaven, M. C. *Adv. Ser. Phys. Chem.* **2001**, *11*, 138.
(10) Perram, G. P. *Int. J. Chem. Kinet.* **1995**, *27*, 817.
(11) Palla, A. D.; Carroll, D. L.; Verdeyen, J. T.; Solomon, W. C. *J. Appl. Phys.* **2006**, *100*, 023117.
(12) Zolotarev, V. A.; Ishkov, D. V.; Podmar'kov, Y. P.; Frolov, M. P.; Yuryshev, N. N. *Sov. J. Quantum Electron.* **1991**, *18*, 912.
(13) Zolotarev, V. A.; Kryukov, P. G.; Podmar'kov, Y. P.; Frolov, M. P.; Yuryshev, N. N. *Sov. J. Quantum Electron.* **1989**, *16*, 1095.
(14) Zolotarev, V. A.; Kryukov, P. G.; Podmar'kov, Y. P.; Frolov, M. P.; Yuryshev, N. N. *Manufacture of Singlet Oxygen*; P. N. Lebedev Physical Institute: Moscow, USSR; Application SU 1668288.
(15) Azyazov, V. N.; Antonov, I. O.; Ruffner, S.; Heaven, M. C. *Proc. SPIE-Int. Soc. Opt. Eng.* **2006**, *6101*, 531.
(16) Payne, W. A.; Thorn, R. P., Jr.; Nesbitt, F. L.; Stief, L. J. *J. Phys. Chem. A.* **1998**, *102*, 6247.
(17) Baulch, D. L.; Cox, R. A.; Crutzen, P. J.; Hampson, R. F.; Kerr, J. A.; Troe, J.; Watson, R. T. *J. Phys. Chem. Ref. Data* **1982**, *11*, 327.
(18) Marx, W.; Bahe, F.; Schurath, U. *Ber. Bunsen-Ges. Phys. Chem.* **1979**, *83*, 225.
(19) Lam, L.; Hastie, D. R.; Ridely, B. A.; Schiff, H. I. *J. Photochem.* **1981**, *15*, 119.
(20) Nishida, S.; Takahashi, K.; Matsumi, Y.; Tanigushi, N.; Hayashida, S. *J. Phys. Chem. A* **2004**, *108*, 2451.
(21) Atkinson, R.; Baulch, D. L.; Cox, R. A.; Hampson, R. F., Jr.; Kerr, J. A.; Rossi, M. J.; Troe, J. *J. Phys. Chem. Ref. Data* **1997**, *26*, 1329.
(22) Gonzales, M.; Valero, R.; Anglada, J. M.; Sayos, R. *J. Chem. Phys.* **2001**, *115*, 7015.
(23) Wayne, R. P. *J. Photochem.* **1984**, *25*, 345.
(24) Zimmerman, J. W.; King, D. M.; Palla, A. D.; Verdeyen, J. T.; Carroll, D. L.; Laystrom, J. K.; Benavides, G.; Woodard, B. S.; Solomon, W. C.; Rawlins, W. T.; Davis, S. J.; Heaven, M. C. *Proc. SPIE-Int. Soc. Opt. Eng.* **2006**, *6261*, 62611R.
(25) Turnipseed, A. A.; Gilles, M. K.; Burkholder, J. B.; Ravishankara, A. R. *Chem. Phys. Lett.* **1995**, *242*, 427.
(26) Jones, I. T. N.; Wayne, R. P. *Proc. R. Soc. London, Ser. A* **1971**, *8*, 259.
(27) Atkinson, R.; Baulch, D. L.; Cox, R. A.; Crowley, J. N.; Hampson, R. F.; Hynes, R. G.; Jenkin, M. E.; Rossi, M. J.; Troe, *J. Atmos. Chem. Phys.* **2004**, *4*, 1461.
(28) Brown, T. J.; Streit, G. E.; Howard, C. J. *J. Chem. Phys.* **1973**, *69*, 1213.
(29) Tellinghuisen, J.; Phillips, L. F. *J. Phys. Chem.* **1986**, *90*, 5108.
(30) Han, J.; Komissarov, A. V.; Tinney, S. P.; Heaven, M. C. *Proc. SPIE-Int. Soc. Opt. Eng.* **2003**, *4971*, 45.
(31) Atkinson, R.; Baulch, D. L.; Cox, R. A.; Crowley, J. N.; Hampson, R. F.; Hynes, R. G.; Jenkin, M. E.; Kerr, J. A.; Rossi, M. J.; Troe, J. *http://www.iupac-kinetic.cam.ac.uk/*. (accessed March 2005).
(32) Sun, F.; Glass, G. P.; Curl, R. F. *Chem. Phys. Lett.* **2001**, *337*, 72.
(33) Newman, S. M.; Lane, I. C.; Orr-Ewing, A. J. *J. Chem. Phys.* **1999**, *110*, 10749.
(34) Komissarov, A. V.; Heaven, M. C. *J. Phys. Chem. A* **2003**, *107*, 10527.
(35) Roszak, S.; Krauss, M.; Alekseyev, A. B.; Liebermann, H. P.; Buenker, R. J. *J. Phys. Chem. A* **2000**, *104*, 2999.
(36) Vasiljeva, A. N.; Klopovskiy, K. S.; Kovalev, A. S.; Lopaev, D. V.; Mankelevich, Y. A.; Popov, N. A.; Rakhimov, A. T.; Rakhimova, T. V. *J. Phys. D: Appl. Phys.* **2004**, *37*, 2455.